

Silencing PPAP2C inhibits lung adenocarcinoma migration and invasion via the ERK/JNK pathway

YI LI^{1*}, WENHUI DANG^{2*}, TING JIAO², MENG Ying ZHANG² and WEI LI²

¹Department of Electrocardiography, Baoji Hospital of Traditional Chinese Medicine, Baoji, Shaanxi 721000, P.R. China;

²Department of Respiratory and Critical Care Medicine, Second Affiliated Hospital of Xi'an Jiaotong University, Xi'an, Shaanxi 710000, P.R. China

Received July 10, 2024; Accepted October 11, 2024

DOI: 10.3892/mmr.2024.13392

Abstract. Lung adenocarcinoma (LUAD) is a leading cause of cancer-related death due to its aggressive nature and metastatic potential. The present study aimed to explore the expression of phospholipid phosphatase 2 (PPAP2C) in LUAD, and its effect on cell migration and invasion, with a particular focus on its association with the ERK/JNK signaling pathway and epithelial-mesenchymal transition (EMT). The expression of PPAP2C in LUAD was analyzed using data from The Cancer Genome Atlas database. Pearson's correlation coefficient analysis was used to assess the correlation between PPAP2C and genes such as MAPK1, MAPK3, MAPK8, CDH1, CDH2 and SNAI1. Subsequently, the PPAP2C gene was silenced in A549 and H1299 LUAD cell lines using siRNA vectors, followed by assessments of gene expression, cell migration, invasion and protein interaction using reverse transcription-quantitative PCR, western blotting, wound healing assay, Transwell invasion assay, molecular docking analysis, co-immunoprecipitation and immunofluorescence staining. The results showed that PPAP2C was significantly upregulated in LUAD tissues compared with that in normal tissues. In addition, high levels of PPAP2C were significantly correlated with MAPK3, MAPK8, CDH1 and SNAI1. Notably, PPAP2C silencing significantly inhibited cell migration and invasion. Additionally, it reduced the phosphorylation levels of ERK and JNK proteins. PPAP2C showed specific binding sites with ERK1, and co-precipitated with ERK1 in both A549 and H1299 cells. Furthermore, PPAP2C silencing decreased the expression levels of N-cadherin and Snail, while increasing

E-cadherin expression, thereby inhibiting EMT. In conclusion, PPAP2C may be highly expressed in LUAD tissues, and could promote cell migration and invasion by activating the ERK/JNK signaling pathway and inducing EMT. These findings provide a novel potential target for the diagnosis and treatment of LUAD.

Introduction

Lung adenocarcinoma (LUAD) is a major histological subtype of non-small cell lung cancer, accounting for 35-40% of all patients with lung cancer worldwide (1,2). Despite advances in treatment, LUAD continues to pose significant health challenges due to its high rates of tumor invasion, metastasis and recurrence after treatment (3). The etiology of LUAD is multifactorial, involving genetic susceptibility, environmental factors (such as smoking and air pollution) and various gene mutations (4). Current treatment modalities for LUAD include surgical resection, radiotherapy, chemotherapy and targeted therapy (5). Studies using single-cell RNA-sequencing technology have shown that RAC1 serves a critical role in promoting the brain metastasis of LUAD (6). Additionally, circulating tumor DNA methods can detect and analyze the early dissemination of metastasis in LUAD (7). However, despite significant progress, there remain challenges in fully understanding the molecular mechanisms driving LUAD metastasis. Particularly, the role of specific genes and pathways in this process remains poorly understood, which hampers the development of more effective therapeutic strategies.

The phospholipid phosphatase 2 (PPAP2C) gene, also known as PLPP2, serves a critical role in phospholipid metabolism by catalyzing the conversion of phosphatidic acid (PA) to diacylglycerol, a key step in cellular signaling (8,9). Research has indicated that PPAP2C can promote the proliferation of LUAD cells by regulating the synthesis of lipid rafts (10). Epithelial-mesenchymal transition (EMT) is a process of cellular phenotypic transformation where epithelial cells lose cell-cell adhesion and acquire mesenchymal characteristics, resulting in enhanced cell migration and invasion (11). Furthermore, overexpression of PPAP2C has been shown to promote the development of breast cancer by affecting the expression of CDC34, LSM7 and SGTA in EMT-related

Correspondence to: Dr Wei Li, Department of Respiratory and Critical Care Medicine, Second Affiliated Hospital of Xi'an Jiaotong University, 157 Xi Wu Road, Xi'an, Shaanxi 710000, P.R. China
E-mail: liweihuxi@163.com

*Contributed equally

Key words: lung adenocarcinoma, phospholipid phosphatase 2, ERK/JNK signaling pathway, epithelial-mesenchymal transition, cell migration

pathways (8). Despite these insights, the specific role of PPAP2C in LUAD cell metastasis remains unclear.

The ERK and JNK pathways, which are MAPK signaling pathways, regulate gene expression and cellular behavior by activating specific protein kinases, leading to the phosphorylation of downstream target proteins (12). The ERK pathway is typically activated by the Ras-Raf-MEK-ERK signaling cascade, whereas the JNK pathway is activated by MAP3Ks, MKK4/7 and JNK (13). The ERK/JNK pathways have critical roles in various cellular processes, such as proliferation, differentiation, apoptosis and stress responses (14). Research has shown that overexpression of Notch4 may enhance the activities of ERK, JNK and p38, thereby promoting the proliferation, anti-apoptosis and migratory abilities of LUAD cells (15). Currently, the association between PPAP2C and the ERK/JNK pathways in LUAD is unexplored, creating a significant gap in the understanding of LUAD metastasis.

Given these challenges, the present study aimed to systematically investigate the function of PPAP2C in LUAD, focusing on its impact on the ERK/JNK signaling pathways and the EMT process, thereby identifying novel potential therapeutic targets for LUAD. By silencing the PPAP2C gene, its specific effects on LUAD cell migration, invasion and related signaling pathways were explored, providing new potential targets and a theoretical basis for the diagnosis and treatment of LUAD.

Materials and methods

Database analysis. Data analysis was performed using R software (version 4.2.1; <https://www.r-project.org>) with packages including ggplot2 (version 3.3.6; <https://ggplot2.tidyverse.org>), stats (version 4.2.1) and car (version 3.1-0; <https://cran.r-project.org/web/packages/car/index.html>). Statistical analysis was carried out using the stats and car packages specifically tailored to accommodate the structured and quantitative nature of the data type. RNA-sequencing data from The Cancer Genome Atlas (TCGA)-LUAD project were downloaded and processed from TCGA database (<https://portal.gdc.cancer.gov>), by extracting TPM-formatted data following the STAR pipeline (16). The data were $\log_2(\text{value}+1)$ -transformed and the expression differences of PPAP2C (ENSG00000141934.10) between tumor and normal tissue samples were evaluated using the Wilcoxon rank-sum test. Visualization was performed using the ggplot2 package. Additionally, patients were divided based on the median expression level of PPAP2C. Those with expression levels above the median were classified as 'high expression,' and those below as 'low expression.' This method ensures a balanced distribution of patients across both groups, facilitating more robust statistical comparisons. Co-expression heatmaps were generated through Pearson's correlation coefficient analysis to assess the correlation of PPAP2C with other genes (MAPK1, MAPK3, MAPK8, CDH1, CDH2 and SNAI1).

Cell culture. A549 (cat. no. CL-0016; Wuhan Pricella Biotechnology Co., Ltd.) and H1299 (cat. no. CL-0165; Wuhan Pricella Biotechnology Co., Ltd.) cells were cultured in Dulbecco's modified Eagle's medium (DMEM; cat. no. 11965-092) containing 10% fetal bovine serum (FBS; cat. no. 10270-106) and 1% penicillin-streptomycin

solution (cat. no. 15140-122) (all from Gibco; Thermo Fisher Scientific, Inc.). Cells were maintained at 37°C in a humidified atmosphere containing 5% CO₂ (Forma 3110; Thermo Fisher Scientific, Inc.). Upon reaching 80-90% confluence, the cells were trypsinized with 0.25% trypsin-EDTA (cat. no. 25200-072; Gibco; Thermo Fisher Scientific, Inc.) and subcultured at a 1:3 ratio. Cell counting was performed using a TC20 automated cell counter (Bio-Rad Laboratories, Inc.). All experiments were conducted under sterile conditions in a biosafety cabinet (1300 Series A2; Thermo Fisher Scientific, Inc.).

siRNA synthesis and cell transfection. The siRNA targeting the PPAP2C gene (Gene ID: 8612) was synthesized by Guangzhou Anerno Biotechnology Co., Ltd. A scrambled negative control (NC) sequence was also synthesized (Guangzhou Anerno Biotechnology Co., Ltd.). Lipofectamine® 2000 (cat. no. 11668027; Invitrogen; Thermo Fisher Scientific, Inc.) was used as the transfection reagent. Briefly, A549 (cat. no. CL-0016; Wuhan Pricella Biotechnology Co., Ltd.) and H1299 (cat. no. CL-0165; Wuhan Pricella Biotechnology Co., Ltd.) cells were seeded into 6-well plates at a density of 5×10^5 cells/well and were cultured for 24 h to reach 80-90% confluence. For transfection, 4 μ g of the constructed silencing vector DNA was incubated with 10 μ l Lipofectamine 2000 in 250 μ l serum-free medium Opti-MEM (cat. no. 31985062; Gibco; Thermo Fisher Scientific, Inc.) at room temperature for 20 min and was then added to each well containing 2 ml serum-free medium. After incubation at 37°C 6 h of incubation, the medium was replaced with complete medium containing 10% FBS. PPAP2C gene expression levels were detected at 48 h post-transfection by reverse transcription-quantitative PCR (RT-qPCR), and the relative expression levels were calculated using the $2^{-\Delta\Delta C_q}$ method (17). Each experiment was repeated three times, with three technical replicates per experiment, to ensure data reliability and accuracy. The siRNA sequences are presented in Table I.

RT-qPCR. A549 and H1299 cells were ground thoroughly in liquid nitrogen, followed by the addition of 1 ml RNAiso Plus (cat. no. 9109; Takara Bio, Inc.), and were mixed thoroughly by vortexing, then placed on ice for 5 min. Subsequently, 0.2 ml chloroform (cat. no. C805077; Shanghai Macklin Biochemical Co., Ltd.) was added, shaken vigorously for 15 sec and incubated at 4°C for 3 min. After centrifugation (D-1524R; Zhuhai Hema Medical Instrument Co., Ltd.) at 1,969 x g for 15 min at 4°C, the aqueous phase was transferred to a new tube. An equal volume of isopropanol (cat. no. H920368; Shanghai Macklin Biochemical Co., Ltd.) was then added, mixed well and incubated at -20°C for 20 min, followed by centrifugation at 1,969 x g for 15 min at 4°C. The supernatant was discarded, and the pellet was washed with 1 ml 75% DEPC-treated ethanol (cat. no. H855322 Shanghai Macklin Biochemical Co., Ltd.) and then centrifuged at 875 x g for 5 min at 4°C. The liquid was discarded, and the pellet was air-dried at room temperature. RNA was dissolved in 30 μ l DEPC-treated ddH₂O (cat. no. W915679 Shanghai Macklin Biochemical Co., Ltd.) and stored at -80°C. RNA concentration was measured using a Q6000UV UV spectrophotometer

Table I. Sequences of siRNAs and primers.

ID	Sequence (5'-3')
si-PPAP2C #1	Sense: CCCCUGACAAGCGAGGAUUUU Antisense: AAAAUCCUCGCUUGUACGGGG
si-PPAP2C #2	Sense: CCCCUGACAAGCGAGGAUUUUA Antisense: UAAAAUCCUCGCUUGUACGGG
si-PPAP2C #3	Sense: CCCC AAAUAUCCCCUUCUUUU Antisense: AAAAGAAGGGGAUAUUUUGGGG
si-NC	Sense: UUCUCCGAACGAGUCACGUUU Antisense: AAACGUGACUCGUUCGGAGAA
PPAP2C	F: CTGCCCTTCGCTATCCTGAC R: CCGTGGGTGATGGTATCTGG
Fos	F: CAAGCGGAGACAGACCAACT R: GTGAGCTGCCAGGATGAACT
Jun	F: GAGACAAGTGGCAGAGTCCC R: TCTTCTCTTGCCTGGCTCTC
GAPDH	F: GACCACAGTCCATGCCATCA R: CCGTTCAGCTCAGGGATGAC

F, forward; NC, negative control; PPAP2C, phospholipid phosphatase 2; R, reverse; si, small interfering.

(Quawell Technology). For cDNA synthesis, 2 μ g total RNA was used as a template, according to the instructions of the Bestar™ qPCR RT Kit (cat. no. 2220; DBI), with a total reaction volume of 10 μ l. qPCR was performed using Bestar™ SybrGreen qPCR MasterMix (cat. no. 2043; DBI) in a final reaction volume of 20 μ l. Fluorescence qPCR experiments were conducted on an Agilent Stratagene fluorescence qPCR instrument (Mx3000P; Stratagene; Agilent Technologies, Inc.). Thermocycling conditions for qPCR included: 95°C for 2 min for initial denaturation, followed by 40 cycles of 95°C for 10 s for denaturation, and 60°C for 30 s for annealing/extension. Results were processed using the $2^{-\Delta\Delta C_q}$ method, with the data presented as the mean \pm standard deviation. Detailed primer sequences are provided in Table I.

Western blot analysis. After washing the cells three times with PBS (cat. no. 14190-144; Thermo Fisher Scientific, Inc.), the samples were centrifuged at 22,000 \times g for 10 min at 4°C using a refrigerated high-speed centrifuge (Zhuhai Hema Medical Instrument Co., Ltd.). The supernatant was collected and stored at -80°C. Proteins were extracted from cells using RIPA lysis buffer (cat. no. P0013B; Beyotime Institute of Biotechnology), containing 1% protease inhibitor cocktail (cat. no. P1005; Beyotime Institute of Biotechnology). Protein concentration was determined using the BCA Protein Assay Kit (cat. no. P0012S; Beyotime Institute of Biotechnology). Protein samples were separated by SDS-PAGE, where the separating gel was prepared by mixing 30% acrylamide (cat. no. 1610156; Bio-Rad Laboratories, Inc.), bis-acrylamide (cat. no. A3574; Sigma-Aldrich), 1.5 mol/l Tris-HCl (pH 8.8; cat. no. MA0053; MeilunBio) and 10% SDS (cat. no. BL517A; Biosharp). A total of 20 μ g of protein was loaded per lane. After polymerization, the stacking gel was added. Following sample loading, electrophoresis was performed using a constant voltage power

supply (DYY-6C; Beijing Liuyi Instrument Factory) at 100 V, and the voltage was increased to 120 V after the samples entered the separating gel, continuing until the bromophenol blue (cat. no. B0126; Sigma-Aldrich) reached the bottom of the gel. After electrophoresis, the proteins were transferred onto a PVDF membrane (cat. no. IPVH00010; MilliporeSigma) using a constant current of 300 mA. The membrane was then washed with TBS buffer (cat. no. T5030; MilliporeSigma) and blocked with 5% non-fat milk (cat. no. A600669; Shanghai Sangon Biotechnology Co., Ltd.) at room temperature for 1 h. The membrane was then incubated with primary antibodies, including anti-PPAP2C (cat. no. PA5-98075; 1:1,200; 33 kDa), anti-phosphorylated (p)-ERK (cat. no. 44-680G; 1:1,000; 42/44 kDa), anti-ERK (cat. no. MA5-15134; 1:1,000; 42/44 kDa), anti-p-JNK (cat. no. 44-682G; 1:1,000; 46/55 kDa), anti-JNK (cat. no. AHO1362; 1:1,000; 46/55 kDa) (all from Thermo Fisher Scientific, Inc.), anti-GAPDH (cat. no. ab9485; 1:2,500; 37 kDa), anti-N-cadherin (cat. no. ab76011; 1:10,000; 125 kDa), anti-E-cadherin (cat. no. ab40772; 1:2,000; 130 kDa) and anti-Snail (cat. no. ab31787; 1:1,000; 68 kDa) (all from Abcam) for 1 h at room temperature. Notably, the band intensity and clarity after 1 h of incubation were comparable to those after overnight incubation. Subsequently, the membranes were incubated with horseradish peroxidase (HRP)-conjugated goat anti-rabbit IgG secondary antibody (cat. no. ab6721; 1:10,000; Abcam) or HRP-conjugated rabbit anti-rat IgG secondary antibody (cat. no. ab6734; 1:2000; Abcam) for 40 min at room temperature. Detection was performed using a chemiluminescence substrate (cat. no. WBKLS0500; MilliporeSigma), and the results were recorded on X-ray film (Guangxi Superstar Medical Device Co., Ltd.) and were analyzed using ImageJ software (version 1.53; National Institutes of Health). The intensity of each band was normalized to the loading control and background intensity was subtracted to exclude

non-specific signals; the final results were expressed in relative intensity units.

Wound healing assay. Complete medium was prepared using high-glucose DMEM (cat. no. E600003; Sangon Biotech Co., Ltd.), supplemented with 10% premium FBS (cat. no. FBS-P01; Shanghai Excell Biological Technology Co., Ltd.) and 1% penicillin-streptomycin (cat. no. P1400; Beijing Solarbio Science & Technology Co., Ltd.) as per the instructions provided by Sangon Biotech Co., Ltd. Horizontal lines were evenly drawn on the back of a 6-well plate (TCP010006; Guangzhou Jet Bio-Filtration Co., Ltd.) using a fine-tip marker pen, with at least five lines crossing each well to standardize the scratch position. Cells grown to 80% confluence were harvested, the old culture medium was aspirated, and the cells were washed 1-2 times with PBS. Cells were treated with trypsin-EDTA (cat. no. E607001; Shanghai Sangon Biotechnology Co., Ltd.) and gently washed, the trypsin solution was aspirated, and the cells were placed in a 37°C incubator (311; Thermo Fisher Scientific, Inc.) for 2-3 min until the cells became round. Fresh complete medium was added, and a single-cell suspension was prepared using a pipette (cat. no. 7010101033; Dragonlab). The cells were counted, and the cell density was adjusted to 5×10^5 /ml. Subsequently, 1 ml cell suspension (5×10^5 cells/ml) was added to each well of the 6-well plate, ensuring each well reached 80% confluence prior to wounding. Fresh complete medium containing specific siRNA treatments targeting PPAP2C gene (si-PPAP2C #1 and si-PPAP2C #2), along with a scrambled siRNA as a NC (si-NC), was added to the respective treatment groups was added. The cells were cultured for 48 h at 37°C and 5% CO₂. A vertical scratch was made using a pipette tip (PPT221010; Guangzhou Jet Bio-Filtration Co., Ltd.). The cells were washed three times with 2 ml PBS/well to remove the detached cells and were then incubated with 2 ml complete medium containing 10% serum (cat. no. A5256701; Thermo Fisher Scientific, Inc.) at 37°C and 5% CO₂ for 24 h. The cells were observed and images were captured using a light inverted microscope (CKX53; Olympus Corporation), and the wound area was analyzed using Image-Pro Plus software (Ver. 6.0; Media Cybernetics, Inc.). The relative migration rate was calculated by measuring the initial wound size and the wound closure rate after 24 h of incubation, normalized to the control.

Transwell invasion assay. Matrigel (cat. no. 356234; Corning, Inc.) was thawed overnight at 4°C and was mixed with pre-cooled serum-free medium at a 1:15 ratio to prepare the gel solution. Subsequently, 100 µl gel solution was added to the upper chamber of Transwell inserts (8 µm pore size; 24-well format; CP012036; Guangzhou Jet Bio-Filtration Co., Ltd.) and allowed to solidify at 37°C for 2 h. Excess liquid was removed, and 50 µl sterile PBS was added to each well and incubated at 37°C for 30 min to wash away the residual Matrigel. Cells were serum-starved for 12 h before seeding. Cells were trypsinized with 0.25% trypsin-EDTA for 2-3 min until they detached, and the cell density was adjusted to 2×10^5 /ml. Subsequently, 100 µl cell suspension (2×10^4 cells/well) was added to the upper chamber, and 700 µl complete medium containing 10% FBS was added to the lower chamber. The Transwell inserts

were incubated at 37°C in an atmosphere containing 5% CO₂ and 100% humidity for 24 h. The inserts were then removed, the non-invasive cells in the upper chamber were gently wiped away with a cotton swab and the residual Matrigel was removed. The inserts were washed three times with PBS, fixed with 4% paraformaldehyde at room temperature for 20 min, and washed three more times with PBS. The inserts were then stained with 0.1% crystal violet (cat. no. G1062; Beijing Solarbio Science & Technology Co., Ltd.) solution at room temperature for 10 min, washed with running water, and the membrane was removed from the inserts using a scalpel, air-dried and mounted with neutral resin. Slides were scanned, and three random fields were selected for cell counting using a light microscope.

Molecular docking experiment. First, the X-ray crystal structure of ERK1 was obtained from the Protein Data Bank (PDB) with the PDB ID: 3FHR (<https://www.rcsb.org/structure/3FHR>). The three-dimensional structure of PPAP2C was constructed using AlphaFold (version 2.1.1; <https://alphafold.ebi.ac.uk/>) with default settings. To ensure the accuracy of the molecular docking results, the two protein structures were preprocessed using AutoDockTools-1.5.7 (<https://autodock.scripps.edu/>), including manual removal of water molecules and the addition of polar hydrogens. Subsequently, protein-protein docking simulations were performed using the GRAMM docking server (<https://gramm.compbio.ku.edu/>) with default parameters. The resulting protein complex was further manually optimized with AutoDockTools-1.5.7, where water molecules were again removed, and polar hydrogens were added. Finally, protein-protein interactions were visualized and analyzed using PyMOL (<https://pymol.org/>), generating the corresponding interaction diagrams.

Co-immunoprecipitation experiment. Total proteins were extracted from H1299 and A549 cell lines. The cells were washed three times with PBS and lysed using RIPA lysis buffer containing protease inhibitors (cat. no. P0013B; Beyotime Institute of Biotechnology). The lysates were centrifuged at 22,000 x g for 10 min at 4°C using a refrigerated high-speed centrifuge (TGL-16M; Zhuhai Hema Medical Instrument Co., Ltd.) and the supernatant was collected. PPAP2C antibody (cat. no. ab168371; 1:10,000; 36 kDa; Abcam) was added to the cell lysates and incubated overnight at 4°C to ensure sufficient binding. As a control, IgG (cat. no. ab18443; 1:10,000; Abcam) was used in a parallel experiment under the same conditions. A total of 50 µl protein A/G magnetic beads (cat. no. 10002D; Thermo Fisher Scientific, Inc.) were then added, and the mixture was incubated for an additional 2 h at 4°C to capture the antibody-antigen complexes. After incubation, the immune complexes were collected by centrifugation at 22,000 x g for 10 min at 4°C and washed three times with lysis buffer. The washed beads were suspended in SDS loading buffer (cat. no. P0015F; Beyotime Institute of Biotechnology) and heated to 95°C to elute the proteins from the beads. The resulting protein samples underwent western blotting, as aforementioned, using a 12% SDS-PAGE gel. The membrane was probed with an anti-ERK1 antibody (cat. no. ab32537; 1:1,000; 43 kDa; Abcam) followed by an HRP-conjugated secondary

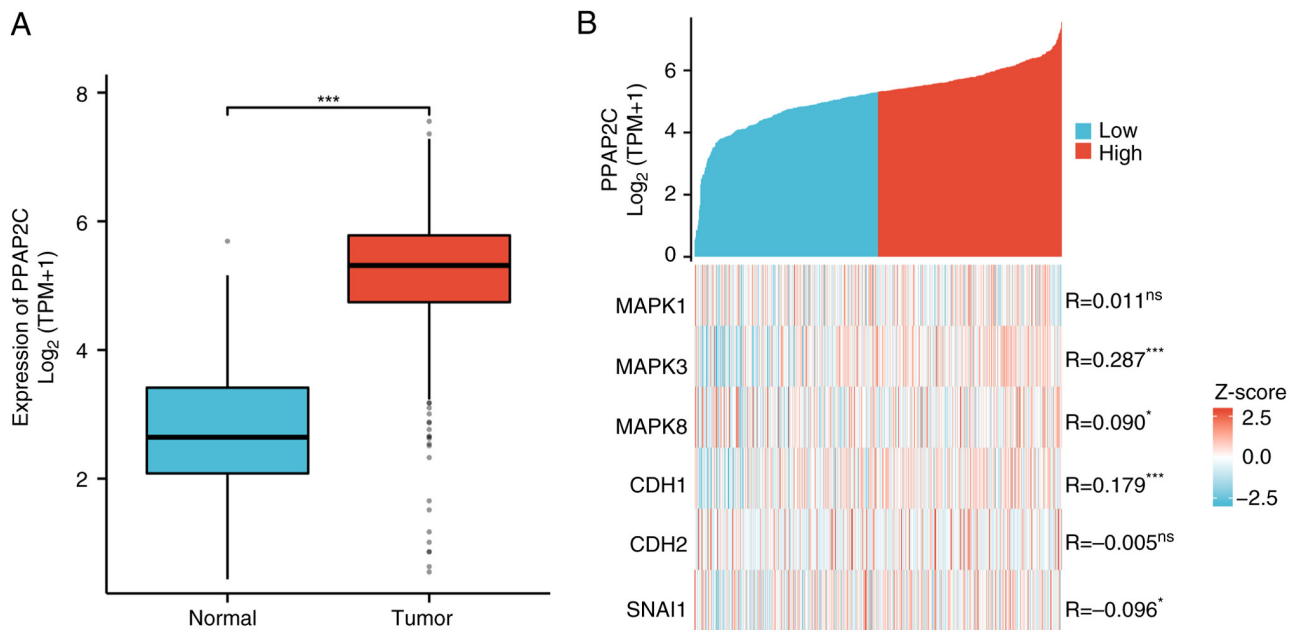


Figure 1. High expression of PPAP2C in LUAD, and its correlation with the ERK/JNK pathway and EMT-related genes. (A) Expression levels of PPAP2C were compared between normal tissues (n=59) and LUAD tissues (n=539). (B) Correlation between PPAP2C expression levels and the expression of genes, including MAPK1, MAPK3, MAPK8, CDH1, CDH2 and SNAI1, in groups with high and low PPAP2C expression. The comparison of PPAP2C expression levels between normal and LUAD tissues was conducted using the Wilcoxon rank-sum test. * $P<0.05$, *** $P<0.001$. LUAD, lung adenocarcinoma; ns, not significant; PPAP2C, phospholipid phosphatase 2.

antibody (cat. no. ab6721; 1:10,000; Abcam) at room temperature for 1 h each. Finally, detection was performed using a chemiluminescence substrate and the results were recorded using medical X-ray film.

Immunofluorescence staining. Cells were fixed with 4% paraformaldehyde for 20 min at room temperature, washed three times with 1 ml PBS, and permeabilized with 0.1% Triton X-100 for 10 min at room temperature, followed by three washes with 1 ml PBS. The cells were then incubated overnight at 4°C with primary antibodies against E-cadherin (cat. no. ab40772; 1:1,000; Abcam), followed by incubation with Alexa Fluor 488-conjugated secondary antibodies (cat. no. A-21206; 1:1,000; Thermo Fisher Scientific, Inc.) for 1 h at room temperature. Nuclei were stained with DAPI (cat. no. D1306; 1:1,000; Thermo Fisher Scientific, Inc.) for 5 min at room temperature, followed by three washes with 1 ml PBS, and the cells were observed and images were captured using an inverted fluorescence microscope (CKX53; Olympus Corporation).

Statistical analysis. Statistical analysis and data visualization were performed using GraphPad Prism 9.0 software (Dotmatics). The normality of the data distribution was assessed using the Shapiro-Wilk test. For data that followed a normal distribution, comparisons between two groups were performed using Student's t-test. For comparisons between two groups not following a normal distribution, the Wilcoxon rank-sum test was used. For comparisons involving multiple groups, one-way ANOVA was used, followed by Tukey's post hoc test to account for multiple comparisons. Data following a normal distribution are presented as the mean \pm standard deviation, while data not following a normal distribution are

expressed as median and IQR. $P<0.05$ was considered to indicate a statistically significant difference.

Results

PPAP2C is highly expressed in LUAD and is correlated with the ERK/JNK pathway and EMT-related genes. The expression levels of PPAP2C were lower in normal lung tissues, from healthy individuals (n=59), and were markedly elevated in LUAD tissues (n=539; $P<0.001$; Fig. 1A). Further analysis demonstrated associations between the expression levels of PPAP2C and the genes MAPK1, MAPK3, MAPK8, CDH1, CDH2 and SNAI1. Specifically, high expression of PPAP2C was associated with MAPK3, MAPK8, CDH1 and SNAI1 ($P<0.05$, $P<0.001$; Fig. 1B).

Successful construction of a PPAP2C gene silencing model in LUAD cells. In A549 cells, RT-qPCR was used to detect the mRNA expression levels of the PPAP2C gene after silencing. The results showed that compared with the si-NC group, all three silencing targets (small interfering RNA: si-PPAP2C#1, si-PPAP2C#2 and si-PPAP2C#3) significantly reduced the mRNA expression levels of PPAP2C, with si-PPAP2C#1 showing the greatest reduction ($P<0.001$; Fig. 2A). The RT-qPCR results in H1299 cells were similar to those in A549 cells, showing significant downregulation of PPAP2C across all three silencing targets, with si-PPAP2C#1 showing the most significant silencing effect ($P<0.001$; Fig. 2B). At the protein level, western blot analysis in A549 cells revealed that PPAP2C protein expression was significantly reduced after silencing, with both the si-PPAP2C#2 and si-PPAP2C#1 groups showing marked downregulation compared with that in the si-NC group ($P<0.01$ and $P<0.001$; Fig. 2C). The results of western

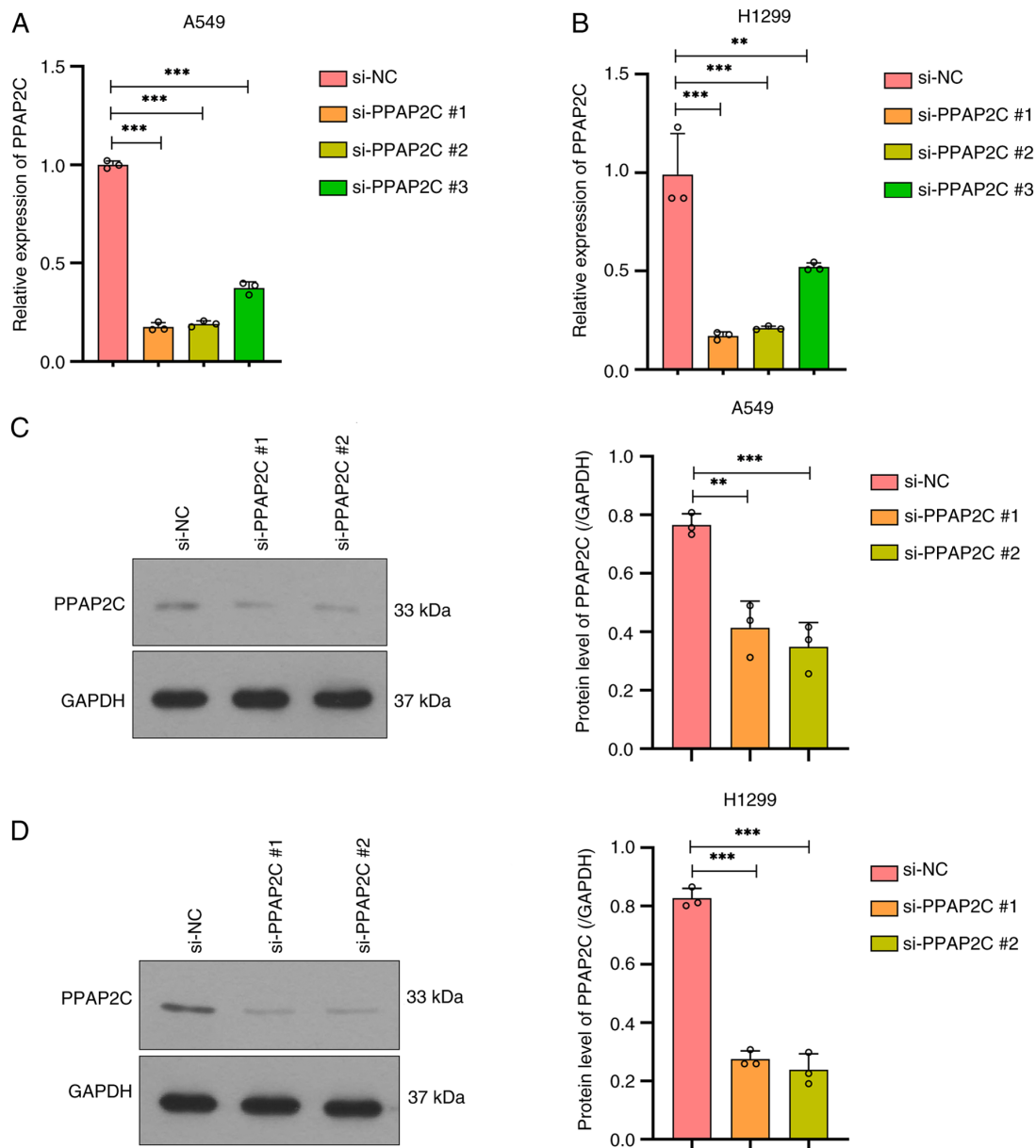


Figure 2. Construction of PPAP2C gene silencing model in lung adenocarcinoma cells. Reverse transcription-quantitative PCR analysis of mRNA expression levels of PPAP2C in (A) A549 and (B) H1299 cells following silencing. Western blot analysis of PPAP2C protein levels in (C) A549 and (D) H1299 cells following silencing. The experiments were repeated three times. ** $P < 0.01$, *** $P < 0.001$. NC, negative control; PPAP2C, phospholipid phosphatase 2; si, small interfering.

blotting in H1299 cells demonstrated a similar trend to that in A549 cells, with a significant reduction in PPAP2C protein expression after silencing, with si-PPAP2C#2 showing the most pronounced downregulatory effect ($P < 0.001$; Fig. 2D). As si-PPAP2C #1 and si-PPAP2C #2 showed the most effective silencing, they were selected for subsequent experiments.

Silencing of the PPAP2C gene inhibits the migration and invasion of LUAD cells. After PPAP2C silencing, the migratory capability of A549 and H1299 cells significantly decreased within 24 h, and the relative migration rate was significantly lower than that of the si-NC group ($P < 0.001$; Fig. 3A). Additionally, the invasive ability of A549 and H1299 cells was markedly reduced after PPAP2C silencing, as evidenced by a significant decrease in the number of

invasive cells per field compared with that in the si-NC group ($P < 0.001$; Fig. 3B).

Silencing of PPAP2C significantly inhibits the activity of the ERK/JNK signaling pathway. Western blot analysis detected the protein expression levels of ERK and JNK, as well as their phosphorylated forms (p-ERK and p-JNK), showing a significant reduction in phosphorylation levels of both ERK and JNK in the si-PPAP2C#1 and si-PPAP2C#2 groups compared with those in the si-NC group ($P < 0.001$; Fig. 4A). The RT-qPCR results indicated that, compared with those in the si-NC group, the mRNA expression levels of the ERK/JNK downstream genes Fos and Jun were significantly reduced in the si-PPAP2C#1 and si-PPAP2C#2 groups ($P < 0.001$; Fig. 4B). Molecular docking results demonstrated that there were clear

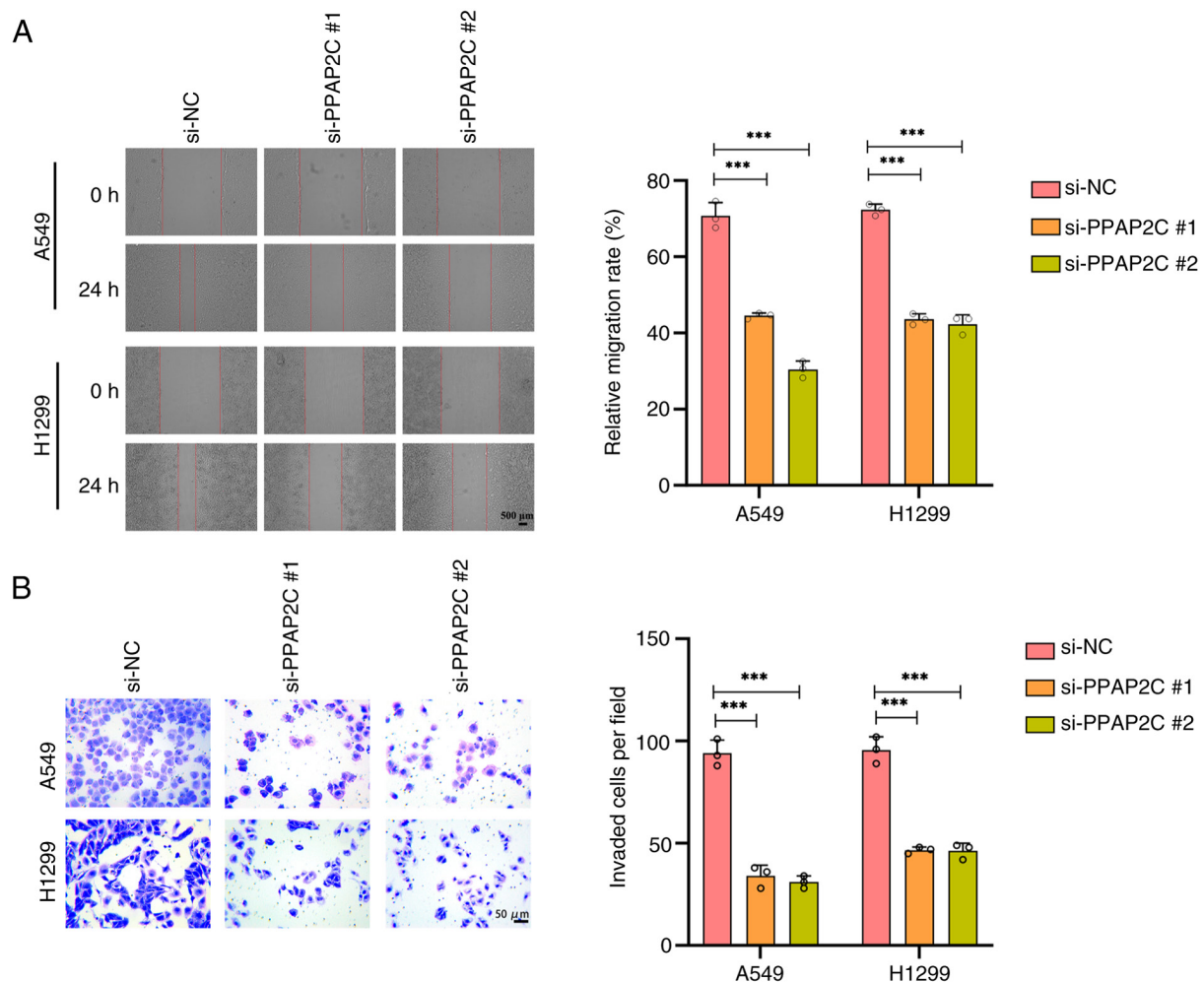


Figure 3: Silencing of PPAP2C significantly inhibits migration and invasion of lung adenocarcinoma cells. (A) Wound healing assay was performed to assess the effect of PPAP2C silencing on the migration of A549 and H1299 cells. (B) Transwell invasion assay was conducted to assess the effect of PPAP2C silencing on the invasion of A549 and H1299 cells. The experiments were repeated three times. *** $P < 0.001$. NC, negative control; PPAP2C, phospholipid phosphatase 2; si, small interfering.

binding sites between PPAP2C and ERK1, involving specific amino acid residues such as LYS-332, ILE-62, GLN-322 and HIS-54 (Fig. 4C). Furthermore, co-immunoprecipitation experiments confirmed the interaction between PPAP2C and ERK1 in both H1299 and A549 cell lines compared with the control IgG ($P < 0.001$; Fig. 4D).

PPAP2C gene silencing inhibits EMT in LUAD cells. Western blot analysis of N-cadherin, E-cadherin and Snail revealed that the protein levels of N-cadherin and Snail were significantly reduced, whereas E-cadherin protein levels were significantly increased in the si-PPAP2C#1 and si-PPAP2C#2 groups compared with those in the si-NC group ($P < 0.001$; Fig. 5A). Immunofluorescence staining further confirmed the elevated expression of E-cadherin in the si-PPAP2C#1 and si-PPAP2C#2 groups, as evidenced by the markedly enhanced fluorescence signal (Fig. 5B).

Discussion

LUAD is the most common subtype of lung cancer that is characterized by high invasiveness and metastatic potential,

which contributes to its high mortality rates despite advancements in diagnosis and treatment (4,18). PPAP2C is a PA phosphatase that exhibits aberrant expression in various tumors, such as LUAD (10) and endometrial cancer (19), and is closely associated with tumor progression and prognosis (10,20). The ERK/JNK pathway serves a critical role in cell proliferation, differentiation, migration and apoptosis, and has been shown to be closely linked to tumorigenesis and development in various types of cancer, such as LUAD and breast cancer (15,21). EMT is a crucial process by which tumor cells acquire invasive and migratory capabilities (22,23). The A549 cell line is derived from human LUAD and harbors a KRAS mutation, making it an ideal model for studying the RAS-ERK pathway. This is because the KRAS mutation activates the ERK signaling pathway, affecting cell proliferation and migration. By contrast, the H1299 cell line is also derived from LUAD but lacks the p53 gene, an important tumor suppressor gene. The absence of p53 simulates common genetic defects found in LUAD (24,25). Therefore, A549 and H1299 cells were used for the present experiments. This study investigated the expression of PPAP2C in LUAD, and its association with the ERK/JNK signaling pathway and

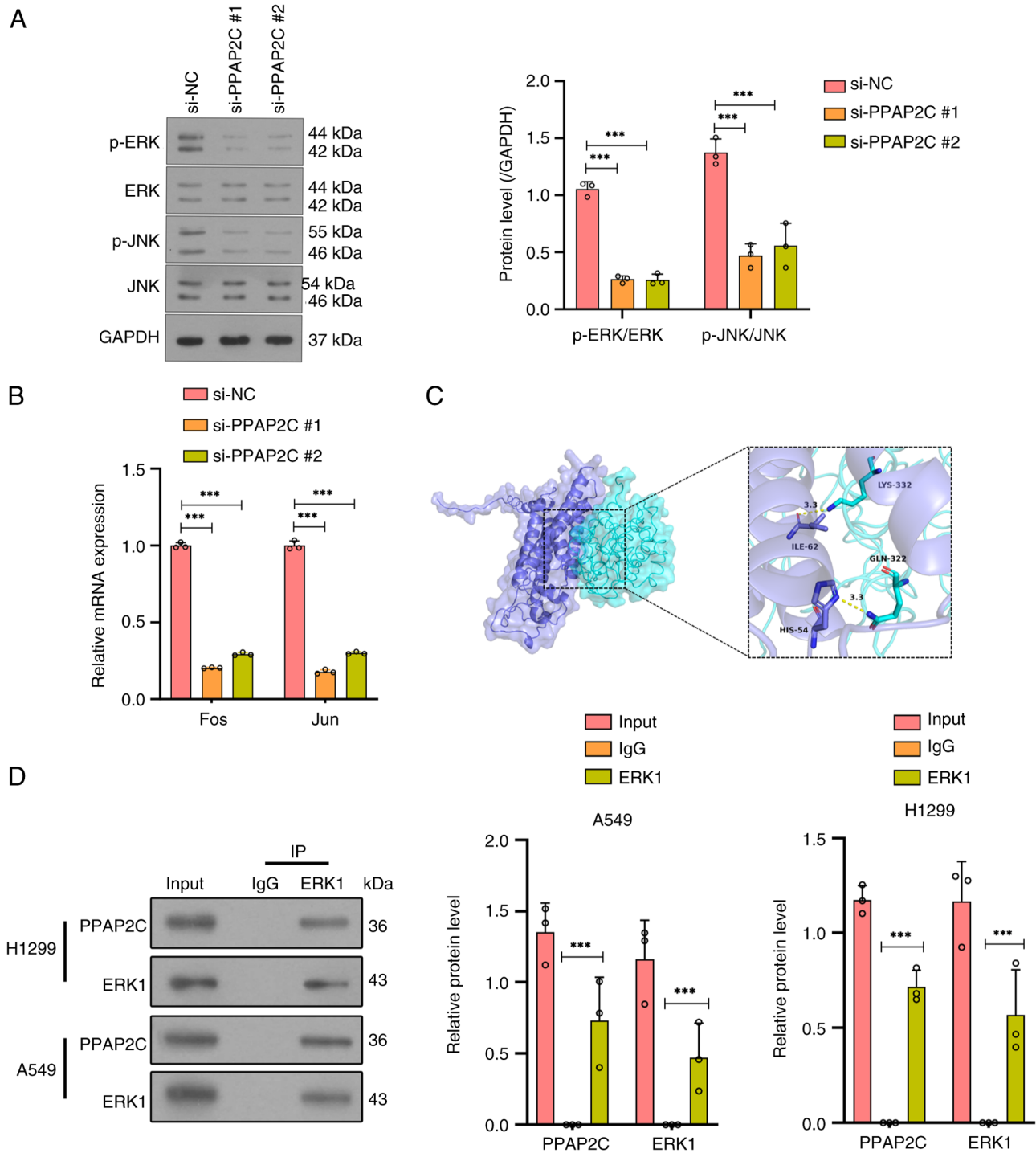


Figure 4. Silencing of PPAP2C significantly inhibits the activity of the ERK/JNK signaling pathway. (A) Western blotting was used to detect the phosphorylation status and total protein levels of ERK and JNK. (B) Reverse transcription-quantitative PCR was used to detect the mRNA expression levels of Fos and Jun genes after PPAP2C silencing. (C) Molecular docking shows the binding sites between PPAP2C and ERK1, PPAP2C is represented as a dark blue model, while ERK1 is depicted as a cyan model. (D) Co-immunoprecipitation was used to detect the interaction between PPAP2C and ERK1. Input refers to the total protein samples that have not undergone co-immunoprecipitation treatment; IgG was used as a negative control. The experiments were repeated three times. *** $P < 0.001$. NC, negative control; p-, phosphorylated; PPAP2C, phospholipid phosphatase 2; si, small interfering; IP, immunoprecipitation.

EMT-related genes, aiming to elucidate the role of PPAP2C in the progression of LUAD.

Previous studies have demonstrated that PPAP2C is highly expressed in various tumors, and its elevated levels are closely associated with increased tumor invasiveness and poor prognosis (8,19). For example, in breast cancer, high expression of PPAP2C can promote cancer cell proliferation

and migration (8). In the present study, it was revealed that PPAP2C was significantly upregulated in LUAD tissues compared with that in normal lung tissues. This finding aligns with previous studies on other types of cancer (20,26), further suggesting that PPAP2C may serve a promotive role in LUAD progression (10), and providing a potential target for a more precise diagnosis and the treatment of LUAD.

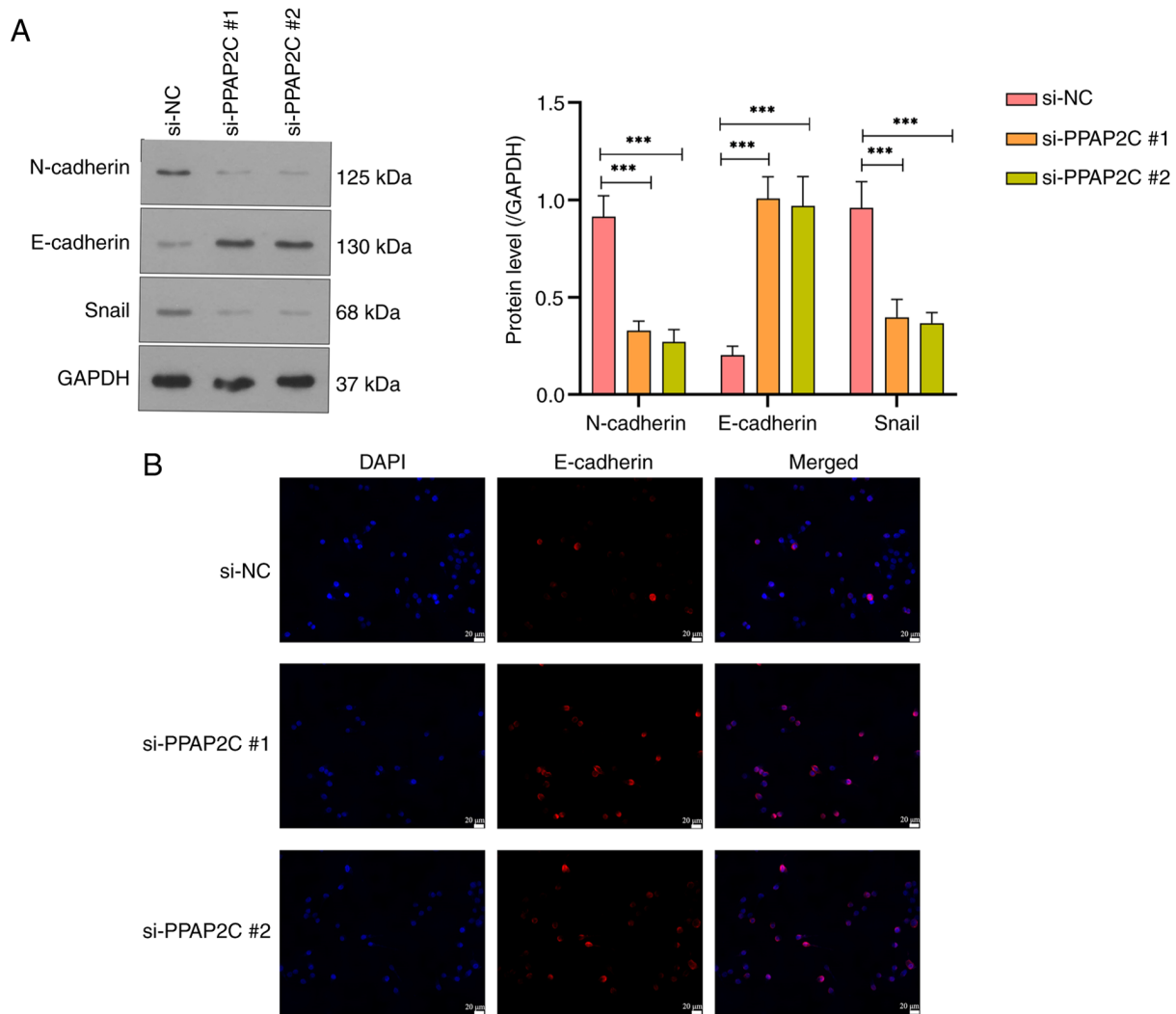


Figure 5. PPAP2C gene silencing inhibits the expression of epithelial-mesenchymal transition markers. (A) Western blot analysis of N-cadherin, E-cadherin and Snail protein levels. (B) Immunofluorescence staining was performed to detect E-cadherin expression and localization in cells; magnification, x400. The experiments were repeated three times. *** $P < 0.001$. NC, negative control; PPAP2C, phospholipid phosphatase 2; si, small interfering.

The ERK/JNK signaling pathway, as a critical branch of the MAPK signaling pathway, has been reported to be aberrantly activated in various types of cancer, such as intrahepatic cholangiocarcinoma (27) and colon cancer (28), promoting tumor cell proliferation and metastasis (14,29). The MAPK1, MAPK3 and MAPK8 genes encode the ERK2, ERK1 and JNK1 proteins, respectively (30,31). Research has shown that inhibiting EMT can significantly reduce the invasiveness of cancer cells (32,33). CDH1, CDH2 and SNAI1 are important genes closely related to EMT. CDH1 encodes E-cadherin, which is primarily expressed in epithelial cells, maintaining cell-cell adhesion and epithelial morphology, while CDH2 encodes N-cadherin, which is mainly expressed in mesenchymal cells, promoting cell migration and invasion (34). SNAI1 encodes the Snail transcription factor, which drives EMT by inhibiting E-cadherin expression and promoting N-cadherin expression (35). It has been demonstrated that PCSK9 promotes EMT and migration of tumor cells in colorectal cancer by upregulating Snail and downregulating E-cadherin (36). The present study revealed that high PPAP2C expression was associated with genes such as MAPK3,

MAPK8, CDH1 and SNAI1, suggesting that PPAP2C may interact with the ERK/JNK pathway and EMT-related genes to promote LUAD progression.

It has been reported that inhibiting the ERK/JNK pathway can significantly reduce the invasiveness and migratory capabilities of tumor cells (37). The present results showed that silencing PPAP2C significantly reduced the migration and invasion of LUAD cells, indicating that PPAP2C may be critical in enhancing the migration and invasion of LUAD cells by modulating key signaling pathways. Although the current study identified the roles of PPAP2C in inhibiting LUAD cell metastasis by silencing the gene, the lack of a pharmacological inhibitor treatment group prevents a comprehensive evaluation of its potential application in clinical therapy. Future research should consider establishing a treatment group using known chemotherapeutic agents as a positive control to confirm the therapeutic efficacy and further clarify the clinical significance of PPAP2C as a potential therapeutic target. Additionally, the absence of a Transwell migration assay may lead to an incomplete understanding of the specific role of PPAP2C in cell migration; therefore, future studies should consider

incorporating this assay to further validate and strengthen the conclusions of this research.

Fos and Jun are key downstream transcription factors of the ERK/JNK signaling pathway, regulated by the activation of ERK and JNK, respectively (38). ERK1/2 can promote cell proliferation by phosphorylating transcription factors, such as c-Fos and Elk-1. Furthermore, JNK1 can regulate gene expression by phosphorylating c-Jun and ATF2, thereby participating in apoptosis and stress responses (39,40). The present study demonstrated that the phosphorylation levels of ERK and JNK were significantly decreased following PPAP2C silencing. PPAP2C silencing also led to a significant reduction in the mRNA expression levels of Fos and Jun genes, further demonstrating that PPAP2C may influence the expression of downstream transcription factors through regulation of the ERK/JNK signaling pathway. Additionally, a clear binding site was identified between PPAP2C and ERK1, and the co-immunoprecipitation assay confirmed their physical interaction in both H1299 and A549 cell lines, further corroborating the interaction between PPAP2C and ERK1. Based on the aforementioned experimental data, it may reasonably be inferred that there is a direct interaction between PPAP2C and ERK1, and this interaction may promote the activation of ERK1. However, these findings are primarily based on *in vitro* cell experiments. Although the results indicated a significant interaction between PPAP2C and ERK1, further *in vivo* studies are needed to validate this mechanism. As there are currently no reports on the specific mechanism by which PPAP2C affects ERK1, to the best of our knowledge, there is no literature to support this finding at present.

The expression of Fra1 is associated with mesenchymal characteristics in epithelial tumors, and it has been shown that dephosphorylated JNK2 can increase Fra1 expression by promoting the expression of c-Jun and Jun-B (41). Additionally, it has been reported that haploinsufficiency of Gata3, a cell cycle inhibitor, in p18Ink4c-deficient mice can upregulate Fra1 and downregulate c-Fos, leading to EMT activation and promoting the initiation and metastasis of breast tumors (42). The present study suggested that PPAP2C may influence EMT through the ERK/JNK signaling pathway. While the current study provides strong evidence that PPAP2C influences EMT markers by modulating the ERK/JNK signaling pathway and its downstream transcription factors Jun and Fos, the exact molecular mechanisms remain unclear. Future research should focus on elucidating the direct target genes regulated by Jun and Fos during EMT, and how PPAP2C modulates these pathways. A deeper understanding of these mechanisms may provide novel therapeutic targets for diseases involving EMT, such as cancer metastasis.

EMT is a critical process by which tumor cells acquire migratory and invasive capabilities, characterized by a decrease in the epithelial marker E-cadherin, and an increase in the mesenchymal markers N-cadherin and Snail (32,43). Studies have shown that modulating the expression of E-cadherin and N-cadherin can significantly impact the invasiveness of tumor cells (44,45). The current study demonstrated that silencing the PPAP2C gene in LUAD cells significantly reduced the protein levels of N-cadherin and Snail, while significantly increasing the protein levels

of E-cadherin. This indicated that PPAP2C may enhance the invasiveness and migratory abilities of LUAD cells by promoting the EMT process. Immunofluorescence staining further confirmed this finding, showing that E-cadherin expression and localization were notably enhanced after PPAP2C silencing. These findings suggested that silencing the PPAP2C gene may reverse the EMT process by restoring E-cadherin expression, and reducing the levels of N-cadherin and Snail, thereby decreasing the invasiveness and migratory capabilities of LUAD cells. Therefore, targeting PPAP2C could be a promising strategy to inhibit EMT and tumor metastasis in LUAD. However, the exact mechanism by which PPAP2C influences EMT has not been fully elucidated in the current study.

Despite the important insights provided by the present study into the critical role of PPAP2C in LUAD, several limitations should be acknowledged. Firstly, the study primarily validated the role of PPAP2C in LUAD through *in vitro* cell experiments, which limits the ability to fully understand the *in vivo* mechanisms of PPAP2C in LUAD progression. Secondly, immunohistochemistry and qPCR experiments were not performed on actual human LUAD tissue samples. Due to the lack of sufficient clinical samples, the expression levels of PPAP2C could not be verified in LUAD tissues and the consistency with the *in vitro* findings could not be assessed. In future studies, we aim to collect and analyze clinical data from patients with LUAD, using survival analysis, multivariate regression analysis and metastasis risk assessment methods to evaluate whether PPAP2C can serve as an independent prognostic marker and a predictor of metastatic risk. Additionally, we aim to explore its relationship with other clinical characteristics, such as tumor staging and treatment response. These studies will help clarify the role of PPAP2C in LUAD progression and provide new insights for personalized treatment. Therefore, future research should consider using animal models and clinical data to more comprehensively validate the key role of PPAP2C in LUAD and to assess its potential as a therapeutic target.

In conclusion, the present study revealed that PPAP2C was highly expressed in LUAD, and could enhance the migration and invasion of LUAD cells by activating the ERK/JNK signaling pathway and promoting the EMT process, thus highlighting its potential as a critical target for therapeutic intervention in LUAD.

Acknowledgements

Not applicable.

Funding

The present study was funded by the Xian Jiaotong University Second Affiliated Hospital Fund for Free Exploration Project [grant no. 2020YJ(ZYTS)086].

Availability of data and materials

The data generated in the present study may be requested from the corresponding author.

Authors' contributions

YL analyzed TCGA data, and conducted the Pearson correlation coefficient analysis, molecular docking and co-immunoprecipitation experiments. WD constructed the PPAP2C gene silencing models, and performed RT-qPCR and western blot analysis. TJ evaluated cell migration and invasion through wound healing and Transwell invasion assays. MZ examined the effects of PPAP2C silencing on the ERK/JNK signaling pathway and EMT using western blotting and immunofluorescence staining. WL supervised the project, contributed to study design and revised the manuscript. YL and WL confirm the authenticity of all the raw data. All authors read and approved the final version of the manuscript.

Ethics approval and consent to participate

Not applicable.

Patient consent for publication

Not applicable.

Competing interests

The authors declare that they have no competing interests.

References

- Su L, Zhao J, Su H, Wang Y, Huang W, Jiang X and Gao S: CircRNAs in Lung Adenocarcinoma: Diagnosis and Therapy. *Curr Gene Ther* 22: 15-22, 2022.
- Wei X, Li X, Hu S, Cheng J and Cai R: Regulation of ferroptosis in lung adenocarcinoma. *Int J Mol Sci* 24: 14614, 2023.
- Song J, Liu W, Wang J, Hao J, Wang Y, You X, Du X, Zhou Y, Ben J, Zhang X, *et al*: GALNT6 promotes invasion and metastasis of human lung adenocarcinoma cells through O-glycosylating chaperone protein GRP78. *Cell Death Dis* 11: 352, 2020.
- Song Y, Kelava L and Kiss I: MiRNAs in lung adenocarcinoma: Role, diagnosis, prognosis, and therapy. *Int J Mol Sci* 24: 13302, 2023.
- Fujikawa R, Muraoka Y, Kashima J, Yoshida Y, Ito K, Watanabe H, Kusumoto M, Watanabe SI and Yatabe Y: Clinicopathologic and genotypic features of lung adenocarcinoma characterized by the international association for the study of lung cancer grading system. *J Thorac Oncol* 17: 700-707, 2022.
- Chen M, Li H, Xu X, Bao X, Xue L, Ai X, Xu J, Xu M, Shi Y, Zhen T, *et al*: Identification of RAC1 in promoting brain metastasis of lung adenocarcinoma using single-cell transcriptome sequencing. *Cell Death Dis* 14: 330, 2023.
- Abbosh C, Frankell AM, Harrison T, Kisistok J, Garnett A, Johnson L, Veeriah S, Moreau M, Chesh A, Chaunzwa TL, *et al*: Tracking early lung cancer metastatic dissemination in TRACERx using ctDNA. *Nature* 616: 553-562, 2023.
- Wang Z, Qi H, Zhang Y, Sun H, Dong J and Wang H: PLPP2: Potential therapeutic target of breast cancer in PLPP family. *Immunobiology* 227: 152298, 2022.
- Sun L, Gao M, Qian Q, Guo Z, Zhu P, Wang X and Wang H: Triclosan-induced abnormal expression of miR-30b regulates fto-mediated m(6)A methylation level to cause lipid metabolism disorder in zebrafish. *Sci Total Environ* 770: 145285, 2021.
- Wang Y, Miao Z, Qin X, Yang Y, Wu S, Miao Q, Li B, Zhang M, Wu P, Han Y and Li B: Transcriptomic landscape based on annotated clinical features reveals PLPP2 involvement in lipid raft-mediated proliferation signature of early-stage lung adenocarcinoma. *J Exp Clin Cancer Res* 42: 315, 2023.
- Zhang J, van der Zon G, Ma J, Mei H, Cabukusta B, Agaser CC, Madunić K, Wuhler M, Zhang T and Ten Dijke P: ST3GAL5-catalyzed gangliosides inhibit TGF- β -induced epithelial-mesenchymal transition via T β RI degradation. *EMBO J* 42: e110553, 2023.
- Kang N, Zhang X, Liu K, Qian Y, Dai Y, Song J, Zheng Y and Ye M: Roles of ERK/JNK in carbon black induced AP-1 cell signaling pathway changes. *Wei Sheng Yan Jiu* 50: 533-538, 2021 (In Chinese).
- Qiu Q, Yu X, Chen Q and He X: Sema3A inactivates the ERK/JNK signalling pathways to alleviate inflammation and oxidative stress in lipopolysaccharide-stimulated rat endothelial cells and lung tissues. *Autoimmunity* 56: 2200908, 2023.
- Zhang Z, Yang Z, Wang S, Wang X and Mao J: Targeting MAPK-ERK/JNK pathway: A potential intervention mechanism of myocardial fibrosis in heart failure. *Biomed Pharmacother* 173: 116413, 2024.
- Li X, Cao X, Zhao H, Guo M, Fang X, Li K, Qin L, He Y and Liu X: Hypoxia Activates Notch4 via ERK/JNK/P38 MAPK signaling pathways to promote lung adenocarcinoma progression and metastasis. *Front Cell Dev Biol* 9: 780121, 2021.
- Dobin A, Davis CA, Schlesinger F, Drenkow J, Zaleski C, Jha S, Batut P, Chaisson M and Gingeras TR: STAR: Ultrafast universal RNA-seq aligner. *Bioinformatics* 29:15-21, 2013.
- Livak KJ and Schmittgen TD: Analysis of relative gene expression data using real-time quantitative PCR and the 2(-Delta Delta C(T)) Method. *Methods* 25: 402-408, 2001.
- Du X, Xue Z, Lv J and Wang H: Expression of the Topoisomerase II Alpha (TOP2A) gene in lung adenocarcinoma cells and the association with patient outcomes. *Med Sci Monit* 26: e929120, 2020.
- Huang H, Cai X, Lin J, Wu Q, Zhang K, Lin Y, Liu B and Lin J: A novel five-gene metabolism-related risk signature for predicting prognosis and immune infiltration in endometrial cancer: A TCGA data mining. *Comput Biol Med* 155: 106632, 2023.
- Li C, Tao Y, Chen Y, Wu Y, He Y, Yin S, Xu S and Yu Y: Development of a metabolism-related signature for predicting prognosis, immune infiltration and immunotherapy response in breast cancer. *Am J Cancer Res* 12: 5440-5461, 2022.
- Liu K, Lu R, Zhao Q, Du J, Li Y, Zheng M and Zhang S: Association and clinicopathologic significance of p38MAPK-ERK-JNK-CDC25C with polyploid giant cancer cell formation. *Med Oncol* 37: 6, 2019.
- Xin W, Zhang J, Zhang H, Ma X, Zhang Y, Li Y and Wang F: CLCA2 overexpression suppresses epithelial-to-mesenchymal transition in cervical cancer cells through inactivation of ERK/JNK/p38-MAPK signaling pathways. *BMC Mol Cell Biol* 23: 44, 2022.
- Cheng Y, Shen Y, Fang Q, Duan S, Wang Y, Dai X and Chen Y: Identification of epithelial-mesenchymal transition-related biomarkers in lung adenocarcinoma using bioinformatics and lab experiments. *Aging (Albany NY)* 15: 11970-11984, 2023.
- Du R, Shen W, Liu Y, Gao W, Zhou W, Li J, Zhao S, Chen C, Chen Y, Liu Y, *et al*: TGIF2 promotes the progression of lung adenocarcinoma by bridging EGFR/RAS/ERK signaling to cancer cell stemness. *Signal Transduct Target Ther* 4: 60, 2019.
- Li Z, Chen X and Yi X: The effects of A549 and H1299 cell-derived exosomes on the proliferation and apoptosis of BEAS-2B cells. *Pharmazie* 76: 379-387, 2021.
- Xu Y, Jin Y, Gao S, Wang Y, Qu C, Wu Y, Ding N, Dai Y, Jiang L and Liu S: Prognostic signature and therapeutic value based on membrane lipid biosynthesis-related genes in breast cancer. *J Oncol* 2022: 7204415, 2022.
- Tang J, Liao Y, He S, Shi J, Peng L, Xu X, Xie F, Diao N, Huang J, Xie Q, *et al*: Autocrine parathyroid hormone-like hormone promotes intrahepatic cholangiocarcinoma cell proliferation via increased ERK/JNK-ATF2-cyclinD1 signaling. *J Transl Med* 15: 238, 2017.
- Lee YS, Kim SY, Song SJ, Hong HK, Lee Y, Oh BY, Lee WY and Cho YB: Crosstalk between CCL7 and CCR3 promotes metastasis of colon cancer cells via ERK-JNK signaling pathways. *Oncotarget* 7: 36842-36853, 2016.
- Guo M, Zhang M, Cao X, Fang X, Li K, Qin L, He Y, Zhao J, Xu Y, Liu X and Li X: Notch4 mediates vascular remodeling via ERK/JNK/P38 MAPK signaling pathways in hypoxic pulmonary hypertension. *Respir Res* 23: 6, 2022.
- Kciuk M, Gielecińska A, Budzinska A, Mojzych M and Kontek R: Metastasis and MAPK Pathways. *Int J Mol Sci* 23: 3847, 2022.

31. Allam EA, Ibrahim HF, Abdulmalek SA, Abdelmeniem IM and Basta M: Coenzyme Q(10) alleviates testicular endocrine and spermatogenic dysfunction induced by high-fat diet in male Wistar rats: Role of adipokines, oxidative stress and MAPK/ERK/JNK pathway. *Andrologia* 54: e14544, 2022.
32. Li Z, Yuan X, Wang B and Gao F: Icariin alleviates transforming growth factor- β 1-induced epithelial-mesenchymal transition by targeting Smad and MAPK signaling pathways. *Am J Transl Res* 12: 343-360, 2020.
33. Gao M, Lai K, Deng Y, Lu Z, Song C, Wang W, Xu C, Li N and Geng Q: Eriocitrin inhibits epithelial-mesenchymal transformation (EMT) in lung adenocarcinoma cells via triggering ferroptosis. *Aging (Albany NY)* 15: 10089-10104, 2023.
34. García-Cuellar CM, Santibáñez-Andrade M, Chirino YI, Quintana-Belmares R, Morales-Bárceñas R, Quezada-Maldonado EM and Sánchez-Pérez Y: Particulate Matter (PM(10)) Promotes Cell Invasion through Epithelial-Mesenchymal Transition (EMT) by TGF- β Activation in A549 Lung Cells. *Int J Mol Sci* 22: 12632, 2021.
35. Huang C, Jing X, Wu Q and Ding K: Novel pectin-like polysaccharide from *Panax notoginseng* attenuates renal tubular cells fibrogenesis induced by TGF- β . *Carbohydr Polym* 276: 118772, 2022.
36. Wang L, Li S, Luo H, Lu Q and Yu S: PCSK9 promotes the progression and metastasis of colon cancer cells through regulation of EMT and PI3K/AKT signaling in tumor cells and phenotypic polarization of macrophages. *J Exp Clin Cancer Res* 41: 303, 2022.
37. Batzorig U, Wei PL, Wang W, Huang CY and Chang YJ: Glucose-Regulated protein 94 mediates the proliferation and metastasis through the regulation of ETV1 and MAPK pathway in colorectal cancer. *Int J Med Sci* 18: 2251-2261, 2021.
38. Yin X, Zhou L, Han F, Han J, Zhang Y, Sun Z, Zhao W, Wang Z and Zheng L: Beta-adrenoceptor Activation by Norepinephrine Enhances Lipopolysaccharide-induced Matrix Metalloproteinase-9 Expression Through the ERK/JNK-c-Fos Pathway in Human THP-1 Cells. *J Atheroscler Thromb* 24: 55-67, 2017.
39. Manios K, Tsiambas E, Stavrakis I, Stamatiopoulos A, Kavantzis N, Agrogiannis G and C Lazaris A: c-Fos/c-Jun transcription factors in non-small cell lung carcinoma. *J BUON* 25: 2141-2143, 2020.
40. Wang Q, Li Z, Wang D, Yang S and Feng Y: Myocardial protection properties of parishins from the roots of *Gastrodia elata* Bl. *Biomed Pharmacother* 121: 109645, 2020.
41. Hu S, Dong X, Gao W, Stupack D, Liu Y, Xiang R and Li N: Alternative promotion and suppression of metastasis by JNK2 governed by its phosphorylation. *Oncotarget* 8: 56569-56581, 2017.
42. Liu X, Bai F, Wang Y, Wang C, Chan HL, Zheng C, Fang J, Zhu WG and Pei XH: Loss of function of GATA3 regulates FRA1 and c-FOS to activate EMT and promote mammary tumorigenesis and metastasis. *Cell Death Dis* 14: 370, 2023.
43. Xu H, Xu WH, Ren F, Wang J, Wang HK, Cao DL, Shi GH, Qu YY, Zhang HL and Ye DW: Prognostic value of epithelial-mesenchymal transition markers in clear cell renal cell carcinoma. *Aging (Albany NY)* 12: 866-883, 2020.
44. Na TY, Schecterson L, Mendonsa AM and Gumbiner BM: The functional activity of E-cadherin controls tumor cell metastasis at multiple steps. *Proc Natl Acad Sci USA* 117: 5931-5937, 2020.
45. Wei J, Wu L, Yang S, Zhang C, Feng L, Wang M, Li H and Wang F: E-cadherin to N-cadherin switching in the TGF- β 1 mediated retinal pigment epithelial to mesenchymal transition. *Exp Eye Res* 220: 109085, 2022.



Copyright © 2024 Li et al. This work is licensed under a Creative Commons Attribution-NonCommercial-NoDerivatives 4.0 International (CC BY-NC-ND 4.0) License.